This article was downloaded by:
On: *22 January 2011*
Access details: *Access Details: Free Access*
Publisher *Taylor & Francis*
Informa Ltd Registered in England and Wales Registered Number: 1072954 Registered office: Mortimer House, 37-41 Mortimer Street, London W1T 3JH, UK

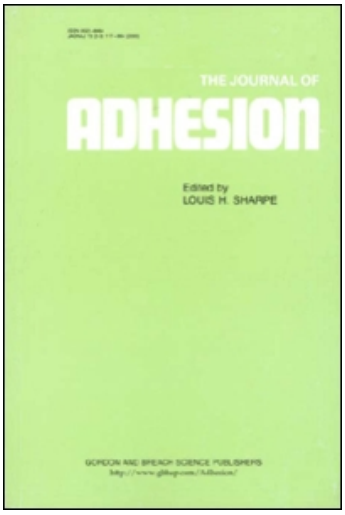

The Journal of Adhesion

Publication details, including instructions for authors and subscription information:
http://www.informaworld.com/smpp/title~content=t713453635

Controlling Adhesion with Surface Hole Patterns

Tina Thomas[a]; Alfred J. Crosby[a]
[a] Polymer Science and Engineering Department, University of Massachusetts, Amherst, Massachusetts, USA

To cite this Article Thomas, Tina and Crosby, Alfred J.(2006) 'Controlling Adhesion with Surface Hole Patterns', The Journal of Adhesion, 82: 3, 311 — 329
To link to this Article: DOI: 10.1080/00218460600646610
URL: http://dx.doi.org/10.1080/00218460600646610

PLEASE SCROLL DOWN FOR ARTICLE

Full terms and conditions of use: http://www.informaworld.com/terms-and-conditions-of-access.pdf

This article may be used for research, teaching and private study purposes. Any substantial or systematic reproduction, re-distribution, re-selling, loan or sub-licensing, systematic supply or distribution in any form to anyone is expressly forbidden.

The publisher does not give any warranty express or implied or make any representation that the contents will be complete or accurate or up to date. The accuracy of any instructions, formulae and drug doses should be independently verified with primary sources. The publisher shall not be liable for any loss, actions, claims, proceedings, demand or costs or damages whatsoever or howsoever caused arising directly or indirectly in connection with or arising out of the use of this material.

The Journal of Adhesion, 82:311–329, 2006
Copyright © Taylor & Francis Group, LLC
ISSN: 0021-8464 print/1545-5823 online
DOI: 10.1080/00218460600646610

Taylor & Francis
Taylor & Francis Group

Controlling Adhesion with Surface Hole Patterns

Tina Thomas
Alfred J. Crosby
Polymer Science and Engineering Department, University of Massachusetts, Amherst, Massachusetts, USA

Defined surface structures of various shapes and length scales can impact the adhesion of polymer interfaces. Most recent research has focused on the use of high-aspect-ratio post-like structures to modify the formation and separation mechanisms for a contacting interface. These mechanisms for controlling adhesion were inspired by the natural mechanisms present in examples such as the gecko and jumping spider. Although post-like structures are effective, numerous other geometries can impact adhesion properties through different mechanisms. In this article, we present and discuss the impact of surface hole patterns on the adhesion of soft, elastomeric interfaces. The surface holes are shallow, cylindrical depressions that decorate the surface of the elastomer and alter the separation mechanisms from rigid surfaces. We specifically focus on the effect of hole radius and nearest hole spacing on the overall adhesion descriptors. Using contact adhesion experiments largely based on the theory of Johnson, Kendall, and Roberts (JKR), we demonstrate that surface holes can alter the stability of the contact edge during interfacial separation. This stability does not affect the overall work of adhesion for a crosslinked polydimethylsiloxane interface, but it does permit tuning of the maximum separation force. These results emphasize the importance of measuring the interfacial area during adhesion testing, the significance of the contact edge, and the opportunities for using surface holes to tune the dissipative processes of interfaces that involve viscoelastic materials. These conclusions are particularly significant in the context of characterization techniques that do not allow for the direct measurement of contact area, such as nanoindentation or scanning probe microscopy measurements.

Keywords: Adhesion; Bio-inspired; Contact; JKR; Pattern; Polymer

Received 26 October 2005; in final form 17 February 2006.
One of a collection of papers honoring Hugh R. Brown, who received the Adhesion Society Award for Excellence in Adhesion Science, sponsored by 3M in February 2006.
Address correspondence to Alfred J. Crosby, Polymer Science and Engineering Department, University of Massachusetts, Amherst, MA 01003, USA. E-mail: crosby@mail.pse.umass.edu

Downloaded At: 08:35 22 January 2011

INTRODUCTION

Inspired by examples such as the gecko and jumping spider, several research groups have demonstrated how micro- and nano-fabricated structures on polymer surfaces can control the adhesion of an interface [1–10]. Most of these structures, because of the inspiration of nature, have a positive skewness (*i.e.* post-like) in which the topography lies generally above the surface baseline (*e.g.*, posts on a surface) (Figure 1). In these cases, the primary mechanism for controlling adhesion is the balance of initiation and propagation events during interfacial separation [8,11,12]. When the pattern features approach length scales that are generally defined by the ratio of G_c/E^*, the mode of local separation is altered and typically increases the overall value of adhesion. Here, G_c is the critical energy-release rate that describes the adhesion of the interface, and E^* is the elastic modulus of the material interface.

Downloaded At: 08:35 22 January 2011

Although post-like patterns produce desirable results, defined surface structures of various shapes can modify adhesion through a variety of mechanisms. In fact, in addition to recent work on post-covered surfaces, several mechanisms were outlined by Kendall in 1975 [13]. For example, Kendall demonstrated how alterations in surface stiffness can control the local separation velocity of a polymer layer, hence controlling the overall adhesion of a viscoelastic polymer. Although the results of Kendall and the recent results of synthetic gecko surfaces demonstrate promise, an understanding of the pattern–material–property relationship has not been developed. In this article, we present our results and discussion on the effect of surface holes on the adhesion of an elastomer to an inorganic surface. The goal of our overall program is to explore the wide parameter space of different patterns and materials with the aim of developing general guidelines for the strategic design and tuning of polymer adhesion.

Surface hole patterns present an interesting case for the geometric control of adhesion. First, the highest topographic level on these surfaces is the continuous phase. In contrast to post-like surfaces where a key mechanism is linked to the mechanical independence of each feature, the mechanical deformation of surface holes is often coupled. This fact immediately suggests that their mechanism for controlling adhesion will be significantly different from that of surface posts. Second, interfacial holes, or cavities, commonly develop during the separation process of many soft polymer interfaces (Figure 1). The experimental results of Creton, Chaudhury, Shull, and others have clearly shown that the onset and propagation of interfacial cavities is a key mechanism related to the overall adhesion of soft polymer

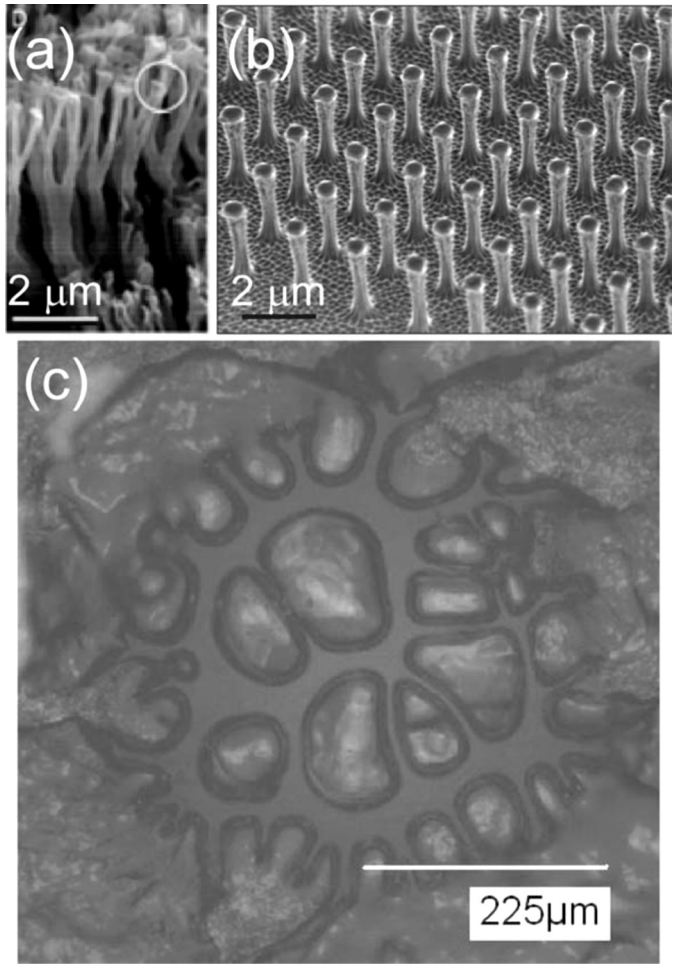

Downloaded At: 08:35 22 January 2011

FIGURE 1 (a) Image of topographic features on the foot of a gecko. Reprinted from Ref. 10. Copyright 2003 National Academy of Sciences, USA. (b) Image of synthetic gecko surfaces. Reprinted by permission from Macmillan Publishers Ltd: *Nature Materials*, (Ref. 5: Geim et al. *Nat. Mater.* **2**, 461–463, 2003). Copyright 2003. (c) Image of cavitated polymer interface during separation.

films [14–19]. Because of the onset of these elastic instabilities, a preferred interfacial geometry develops to increase the overall compliance of the polymer layer and permit chain rotation and motion away from the interface. This chain mobility often enhances energy dissipation, thus increasing the work required to separate the interface. In a related manner, Gay and Leibler [20] described how the

onset of interfacial cavities can cause the development of negative pressures, or vacuum pockets, across a soft polymer interface. Consequently, the energy of separating these interfaces is not only linked to the local material-defined energy-release rate criteria but also to the energy required to overcome the vacuum pressures.

In this article, we discuss how simple patterns of circular surface holes arranged in square arrays can alter the adhesion of crosslinked polydimethylsiloxane to fused silica. We investigate the influence of elastic modulus, hole radius, hole depth, and nearest-neighbor spacing on the separation mechanisms of these interfaces. Our results demonstrate the importance of the contact edge, not the contact area, in defining separation processes and suggest additional mechanisms beyond vacuum development for the control of adhesion. In the following sections, we discuss our experimental approach, an overview of the results, and a discussion of the relationships derived from the response of the patterned interfaces.

Downloaded At: 08:35 22 January 2011

EXPERIMENTAL APPROACH

Pattern Fabrication

To fabricate a patterned layer, we begin with conventional photolithography. We spin coat a commercial photoresist (Shipley SU8 supplied by Microchem Corp., Newton, MA, USA) onto a clean silicon wafer with a thermally grown layer of silicon oxide. After required prebaking of the photoresist, the film is exposed to UV (OAI, 365 nm, OAI, San Jose, CA, USA) through a transparency-printed mask (Pageworks, Cambridge, MA, USA). The exposed photoresist film is subsequently developed to expose a surface of photoresist posts of height (h) equal to the thickness of the spin-coated film. The radius of the posts (r_p) is defined by the mask features. For low-aspect ratios ($h/r_p << 1$), the thickness of the photoresist defines the required height of the surface features, and this photoresist post surface serves as a template for a cured elastomer layer. For deeper pattern features, we wet etch the silicon oxide surface not covered by the photoresist posts. Because of imperfect anisotropic control of wet etching, the posts in the etched silicon oxide display a slight sidewall taper. This taper does not significantly affect the mechanical response of our test samples since we are interested in the cast negative of this post template.

After fabrication of the pattern template, the uncured polymer mixture is poured onto the template, cured, and mechanically released from the rigid template to reveal an elastomer surface with defined surface holes. The mask used in these experiments is designed to

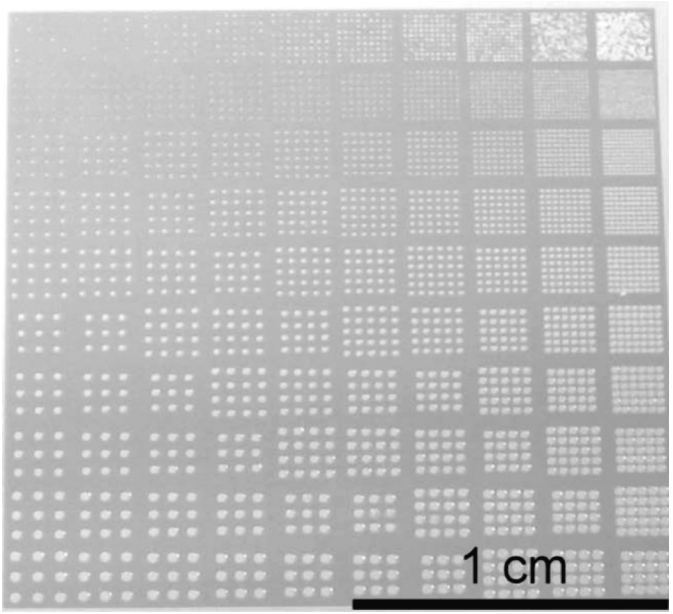

FIGURE 2 Photolithographically fabricated pattern library of holes etched into silicon oxide surface. Diameter of holes varies along vertical axis, and spacing between holes varies along horizontal axis.

Downloaded At: 08:35 22 January 2011

fabricate one surface library with 100 different patterns (Figure 2). Along one axis of the library, the hole radius (r_p) ranges from 25 μm to 250 μm. Along the orthogonal axis, the nearest-neighbor spacing (L) varies from 50 μm to 500 μm. This sample library design ensures equal comparisons of adhesion response across the different patterns. The material properties, history, and overall physical dimensions are conveniently equal with the sample design, thus removing a significant amount of experimental artifact. The depth (h) of the surface holes is either 6 μm or 20 μm for the patterns discussed in this article. The pattern dimensions are reported for specific results.

Materials

The patterned elastomer layers are crosslinked polydimethylsiloxane (PDMS) made from Dow Corning's Sylgard® 184 (Dow Corning, Midland, MI, USA). These products are crosslinked by combining a mixture of crosslinking agent and prepolymer, degassing the mixture to remove air voids, and curing at a constant temperature of 70°C for

2 h. To vary the moduli of this material, we control the ratio of crosslinker to prepolymer from 1:10, 1:15, and 1:20. Because the curing process is not 100% efficient, we swell the cured elastomers in hexane to remove uncrosslinked chains.

The fused silica surface to which the adhesion of the patterned elastomer is measured is a smooth, polished hemisphere of fused silica purchased from ISP Optics Irvington, NY, USA. The radius of curvature (R) of the hemispherical lens is 5 mm.

Contact Adhesion Testing

Contact adhesion testing based on the theory of Johnson, Kendall, and Roberts (JKR) [21] is performed to quantify the adhesion and near-surface mechanical properties of both nonpatterned and patterned surfaces. The details of the instrument and process have been reported previously [11]. In short, the elastomer layer is fixed to a glass slide that is subsequently mounted to the translation stage of an inverted, optical microscope. The fused silica lens then contacts and separates from the elastomer surface while the applied displacement (δ), resultant force (P), and interfacial area ($A = \pi a^2$) are recorded *via* custom-written software in the National Instruments Labview environment (Austin, TX, USA).

Downloaded At: 08:35 22 January 2011

A representative force-displacement curve for a nonpatterned PDMS/fused silica experiment is shown in Figure 3. Corresponding images of the interfacial area are also shown in Figure 3. From these data, we quantify the critical energy-release rate for interfacial separation (G_c) and the elastic modulus (E) of the PDMS near surface. The values of these material and interfacial descriptors for all three PDMS elastomers are provided in Figure 4. The modulus of the elastomer decreases with decreasing weight percent of crosslinking agent due to the decreasing density of crosslink junctions. Also, G_c slightly increases as the weight percent of the crosslinking agent decreases. This behavior is not purely understood because of complex, undisclosed formulation of the commercial PDMS, but these details are not necessary for determining the influence of surface holes on adhesion. We simply use the measured values of G_c and E for nonpatterned surfaces as a baseline for our analysis of patterned surfaces.

The adhesion of patterned surfaces is also measured using the contact adhesion testing method as previously described. Because of the nonaxisymmetric growth of the interfacial area upon contact and separation for these experiments, G_c based on the JKR theory cannot be used as a straightforward descriptor of the patterned interface adhesion. To quantitatively compare the response of surface hole

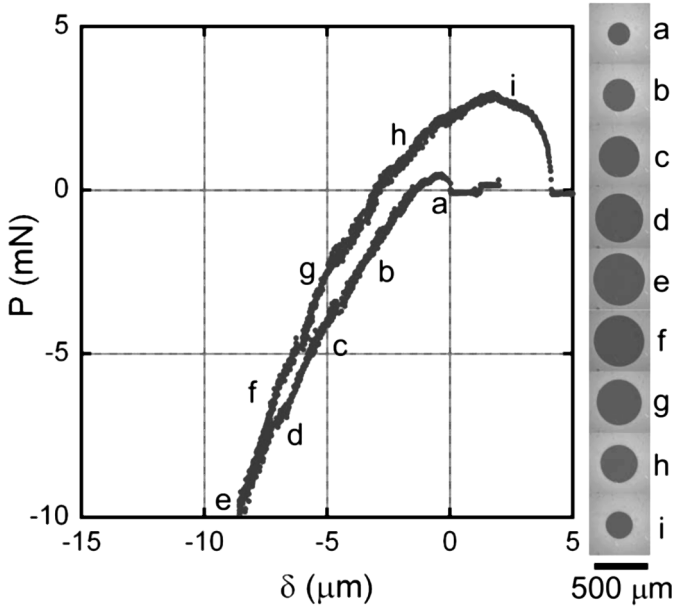

FIGURE 3 Typical force (P) versus displacement (δ) data curve for a glass hemisphere ($R = 5\,\text{mm}$) contacting and separating from a nonpatterned crosslinked PDMS surface. Contact area images as a function of time are shown on right. The crosslinker ratio was 1:10 for this representative sample.

Downloaded At: 08:35 22 January 2011

patterns, we use two adhesion descriptors, W_{adh} and P_{m}. P_{m} is the maximum applied tensile force during separation of an interface. W_{adh} is the overall work of adhesion, or the energy per unit interfacial area that is dissipated between formation and failure of an interface [22]:

$$W_{\text{adh}} = \frac{\oint P d\delta}{A_{\max}} = \frac{2\pi \oint G_{\text{c}} \cdot a \cdot da}{A_{\max}} \tag{1}$$

where $A_{\max}$ is the interfacial area at maximum contact. This descriptor is useful for polymer interfaces whose adhesion is dictated by the history of the interface. For example, for nonpatterned interfaces, these changes may be associated with phenomena such as chemical complexes formed upon contact, rearrangement of surface molecules, or viscous losses in the near-interface molecules [14,23–29].Based on previous research on the adhesion of crosslinked PDMS [26–29], W_{adh} is an appropriate descriptor for this material. This descriptor is not equivalent to the thermodynamic work of adhesion. In fact, for a material interface whose adhesion is only described by reversible,

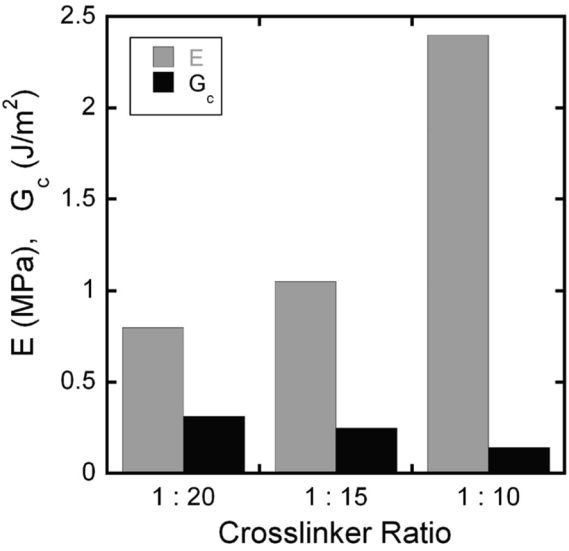

FIGURE 4 Material properties for different formulations of crosslinked PDMS. The elastic modulus (E) and the critical energy release rate (G_c) for separating from a glass surface are presented.

Downloaded At: 08:35 22 January 2011

surface thermodynamics, the value of W_{adh} will equal zero. The data presented here for W_{adh} and P_m represent averages of at least three experiments, and the associated error bars are smaller than the size of the symbols used in the plots.

RESULTS

Upon establishing contact between a spherical probe and surface hole pattern for a given probe curvature and a given maximum force of compression, three behaviors are observed (Figure 5) depending upon the pattern dimensions, the material mechanical properties, and the adhesion forces of the interface. First, the interfacial area is only established on the pattern's top surface, and only one hole (the central hole) is contacted. These experiments are referred to as *single-plane, single-hole contacts*. Second, the interfacial area is only established on the pattern's top surface and multiple holes are contacted at maximum compression. These experiments are referred to as *single-plane, multihole contacts*. The third possibility is that the interfacial area is established on both the top surface and the bottom surface of the hole for only the central hole. These experiments are referred to as *multiplane contacts*.

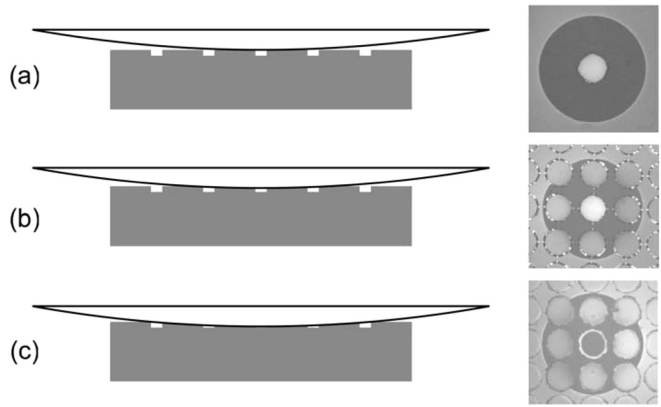

FIGURE 5 Schematic of three different contact scenarios for the contact between a spherical probe and a surface decorated with circular holes. Not drawn to scale. Images on right show true contact area images for different situations. (a) Single-hole contact with established interface surrounding only the central hole. (b) Multiple-hole contact with interface established on only top plane of PDMS surface. (c) Multiple-hole contact with the bottom of the spherical probe contacting the bottom surface of the central hole.

Downloaded At: 08:35 22 January 2011

To organize the results and subsequent discussion, we consider these three experimental observations separately.

Single-Plane, Single-Hole Contacts

Force-displacement curves for contact adhesion experiments on three different hole surfaces with different hole radii (r_p) are shown in Figure 6b. For comparison, the force-displacement curve for a nonpatterned, or smooth, interface is also plotted in Figure 6b for the same material conditions. Although a large fraction of the interfacial area is absent in the three hole contact experiments, the corresponding force-displacement relationship is not altered significantly and generally matches the response of a smooth interface. From Figure 6c it is also clear that the two adhesion descriptors, P_m and W_{adh}, are not significantly affected by the absence of the central interfacial area in the hole contact experiments. Although this result itself is interesting, this observation is particularly significant in the context of characterization techniques that do not allow for the direct measurement of contact area, such as nanoindentation or scanning probe microscopy measurements. For these techniques, the dissipated energy related to adhesion would be normalized by the projected contact area ($A = \pi a^2$)

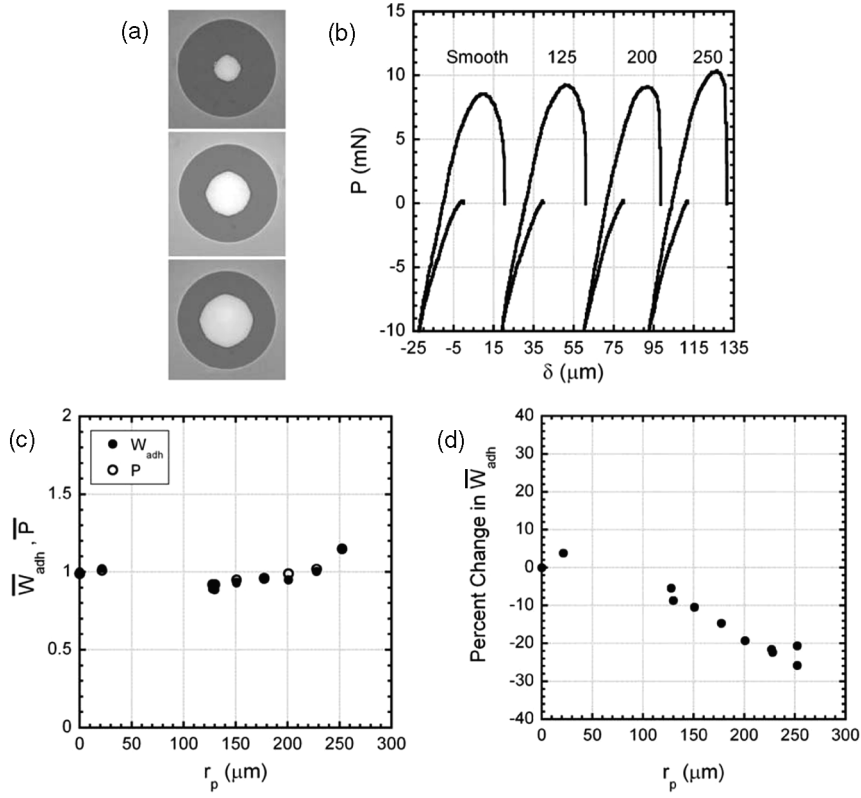

FIGURE 6 Data collected on single-hole, single-plane contact experiments. (a) Contact area images at maximum contact for holes with radii of 125, 200, and 250 μm. (b) Force *versus* displacement curves for nonpatterned surface (left) and three surface holes. Radii of hole displayed above corresponding force-displacement curve. Initial displacement values have been offset for clarity. (c) Normalized W_{adh} and P as a function of hole radius. These values are normalized relative to the corresponding parameter from a nonpatterned interface. (d) Percent change in the overall work of adhesion if a projected contact area is used for analysis. Hole depth (h) equals 20 μm, and the crosslinker ratio was 1:20 for these samples.

as predicted by JKR contact mechanics [21]:

$$a^3 = \frac{3R(1-\nu^2)}{4E}\left(P + 3G\pi R + \sqrt{\{6G\pi RP + (3\pi GR)^2\}}\right) \qquad (2)$$

This projected area would not account for the details of the pattern geometry and would misrepresent the actual interfacial area. If the

Downloaded At: 08:35 22 January 2011

projected contact area was used to calculate W_{adh}, then the calculated values would decrease with increasing radius as shown in Figure 6d. This result points to not only the importance of monitoring the true contact area in adhesion testing but also indicates the influence of the contact edge, not the contact area, in determining the true adhesion response of an interface. This latter point is discussed further in later sections.

Single-Plane, Multihole Contacts

For softer materials and/or patterns with more closely packed features at maximum compression, the interfacial area encompasses multiple-hole features. The force-displacement results and maximum interfacial area images for these cases are shown in Figure 7a. Plotted for comparison is the force-displacement data for a smooth interface from the same materials. Comparing the data in Figure 7a with that in Figure 6a, it is evident that neighboring holes begin to influence the separation process of the elastomer interface. Specifically, force instabilities where the force changes significantly with little change in displacement are evident for multihole interfaces. These sudden changes in the resultant force are attributed to fast transitions in the interfacial area. Essentially, the surface holes pin the contact

Downloaded At: 08:35 22 January 2011

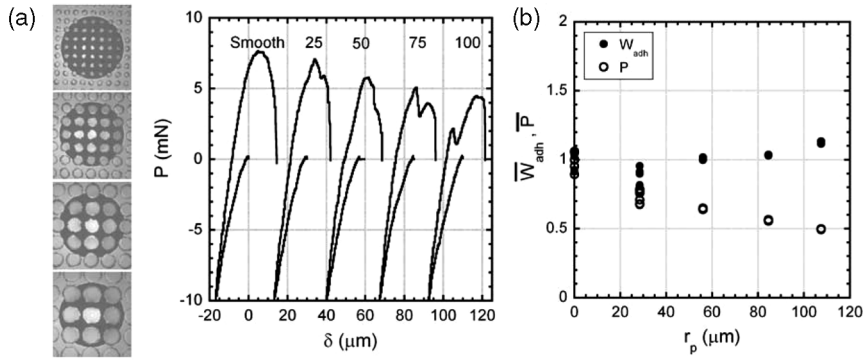

FIGURE 7 Data for multiple-hole, single-plane contact experiments. (a) Maximum contact area images and force-displacement data for surface hole patterns with radii of 25, 50, 75, and 100 μm. Initial displacement values have been offset for clarity. (b) Normalized W_{adh} and P as a function of hole radius. Values are normalized relative to corresponding parameter for nonpatterned interface. Hole depth (h) equals 6 μm, and the crosslinker ratio was 1:15 for these samples.

edge, and upon overcoming a required activation barrier, the contact edge accelerates until a stable propagation is reestablished.

Although these instabilities alter the history of the polymer interface by introducing periods of acceleration, they do not alter W_{adh} in a significant manner (Figure 7b). This lack of influence is largely attributed to the fact that the PDMS interfaces used in these experiments do not display a significant dependence on separation velocity at the length scales probed by our experiments. Therefore, the use of patterns to control local separation velocity has no effect. In contrast to W_{adh}, P_m is altered by the multihole interface. This dependence is clearly shown in Figure 7b where P_m decreases with increasing hole radius.

Multiplane Contacts

Under certain conditions of applied compressive force, hole and probe dimensions, and surface mechanical properties, the bottom surface of a hole is contacted and the interfacial area incorporates two planes. The second plane of contact at the bottom of the hole presents additional mechanisms through which surface holes can alter separation. We observe (Figure 8a) that for isolated hole contacts, P_m increases with increasing hole radius, but W_{adh} and the overall shape of the force-displacement curve for these experiments are unaffected. As multiple holes are incorporated into the interfacial area, the effect of the second plane is diminished and all adhesion descriptors are

Downloaded At: 08:35 22 January 2011

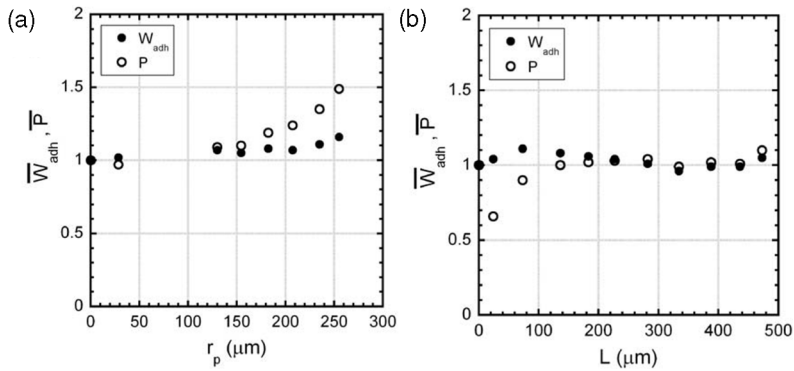

FIGURE 8 (a) Data for single-hole, multiplane contact experiments. Normalized values of W_{adh} and P as a function of hole radius. (b) Data for multiple-hole, multiplane contact experiments. Normalized values of W_{adh} and P as a function of hole edge-to-edge spacing (L). Hole depth (h) equals 6 μm, and the crosslinker ratio was 1:15 for these samples.

relatively unchanged relative to a nonpatterned interface (Figure 8b). Here, the control mechanisms displayed by single-plane contacts dominate the response because our experiments are "single-asperity" contacts, where our spherical probe is the "single-asperity." If multiple-asperity contacts were established, we would expect the trends observed in Figure 8a to continue as multiple holes are contacted.

DISCUSSION

Surface holes can modify or tune adhesion through a wide variety of mechanisms. One obvious mechanism for surface holes is the development of vacuum pockets across the interface. Although this mechanism will significantly enhance the overall energy required for interfacial separation, as discussed by Gay and Leibler [20], it is not the only mechanism presented by surface holes. In our experiments, the development of vacuum pockets is suppressed by the elastic modulus of the PDMS. The material with the lowest modulus value is the 1:20 formulation with an elastic modulus of 0.8 MPa, which is too large to permit the development of vacuum pressures for this geometry. Atmospheric pressure is 0.1 MPa.

Downloaded At: 08:35 22 January 2011

By suppressing this mechanism, our experiments with surface holes provide unique insight into not only surface pattern control of adhesion but also the specific mechanisms of PDMS adhesion. Three primary results are observed in our experiments: 1) contact-area observations are critical for the correct interpretation of adhesion measurements for soft, elastic solids; 2) surface holes can dictate local areas of crack acceleration during separation; and 3) discrete planes of interfacial area can alter the local separation process.

The results presented in Figure 6 clearly demonstrate the importance of the contact area on the interpretation of adhesion measurements. For these measurements, isolated surface holes are contacted with the hemispherical probe, producing the contact areas shown in Figure 6a. These contact areas are axisymmetric, but a large fraction of the internal area is missing because of the presence of the central hole. Although this internal area does not establish an interface, the force-displacement curves produced from these contacts are nearly indistinguishable from the nonpatterned contact. This effect is largely attributed to the contact mechanical response being dictated by the stressed volume of material, which controls the stiffness of the contact geometry. For the surface holes presented in Figure 6, if we consider the outer contact radius to be called a, then the stressed volume will be roughly a^3. Accordingly, the volume fraction of the surface holes in Figure 6 range from 0.014 to 0.058, or less than 6% of the stressed

volume. Because this volume fraction is small and the surface holes are shallow, allowing for the material beneath the hole to contribute mechanically, the stiffness of the interface as described by the force displacement is relatively unaffected.

This similarity in the force-displacement curves is observed for both the loading and unloading portions of the experiments. In the loading portion, all four curves increase in compressive force in a nonlinear manner with $(-\mathrm{P}) \propto (-\delta)^{3/2}$, as predicted by Hertzian contact mechanics. Additionally, the specific path of loading for each hole pattern in Figure 6 can be fit with the following equation:

$$\mathbf{P} = \frac{-4\mathbf{E}}{3(1-\nu^2)}\left(1+\left(\frac{\mathbf{r_p}}{\mathbf{R}}\right)^{\mathbf{n}}\right)\mathbf{R}^{1/2}(-\delta)^{3/2} \tag{3}$$

where n is found to be 1.5 for our experiments. Therefore, the primary effect of the central hole is to modify the stiffness of the near-surface region, and an effective modulus for the near-surface region can be defined as $E_{\mathrm{eff}} = E(1+(r_{\mathrm{p}}/R)^{\mathrm{n}})$. This effect is most dominant at small displacements or when the contact radius is similar to the radius of the hole. Similarly, during the unloading portion of the experiment, the presence of the hole affects the local stiffness at small displacements. This effect does not change the shape of the unloading curve as seen in Figure 6b, but the rate at which force changes increases with increasing hole size.

Although the stressed volume explains the similarity of the force-displacement curves, it also provides insight into the mechanisms of adhesion for crosslinked PDMS interfaces. As Figure 6c demonstrates, the overall energy dissipated ($\overline{W}_{\mathrm{adh}}$) is relatively unaffected by the presence of the hole in the center of the contact area. For Figure 6c, $\overline{W}_{\mathrm{adh}}$ is calculated by normalizing the hysteretic area of the force-displacement curve by the true interfacial area, as measured optically. If the hysteresis processes of this interface were dictated by far-field viscoelastic losses in the elastomer, then $\overline{W}_{\mathrm{adh}}$ would increase with increasing hole radius (Figure 6d). This increase would occur because the stressed volume for the different hole geometries would be nearly identical, and the true interfacial area would decrease significantly for larger holes. Because the true $\overline{W}_{\mathrm{adh}}$ does not depend upon the hole radius, this result strongly indicates that the dissipative processes for the crosslinked PDMS interface are associated with near-interfacial processes, not far-field viscoelastic losses.

This finding is consistent with previous research on the adhesion of crosslinked PDMS and elastomers in general. For crosslinked PDMS

Downloaded At: 08:35 22 January 2011

interfaces, several researchers have shown that a large fraction of the observed hysteresis in contact adhesion experiments is attributed to surface chemical complexes that are formed upon contact [28–30]. Although we cannot definitively attribute our observed hysteresis to similar complexes, the formation of interfacial complexes would lead to the hysteresis corresponding to the interfacial area and not the stressed volume, as observed in Figure 6. These results also support the currently accepted model for the adhesion of weakly viscoelastic elastomer interfaces where the energy dissipation is confined to the near-crack-tip region upon separation [24,25,31,32]. For this model during separation of the elastomer interface, any dissipative processes are isolated to a small volume of material near the crack tip, which experiences the largest stresses. This concept leads to an empirically derived relationship that links the critical energy release rate (G_c) for the interface to the crack-tip velocity, v [25]:

$$G_c = G_o(1 + \kappa(v))(1 + \phi(v)) \tag{4}$$

where $\kappa(v)$ is a dissipative factor related to truly interfacial events and $\phi(v)$ is a dissipative factor related to bulk molecular processes. The dissipative processes described by this empirical model would not be altered by the presence of the surface holes observed in Figure 6; therefore, $\overline{W}_{adh}$ would not depend upon hole size or spacing.

Although the limits are not fully explored in our experiments, these results suggest a surface of defined holes can be an ideal geometry for investigating the length scale of the dissipative region associated with different polymer interfaces. Also, these results demonstrate the importance of observing the contact area directly during the characterization of an interface. With the recent development of using surface probe microscopes (SPM) and nanoindentation instruments to characterize adhesion properties on small length scales, our results clearly demonstrate how the force-displacement curve can be severely misleading without the knowledge of the contact area. Because the ratio of the probe curvature to the length scale of topographic features on a typical surface for these measurements is similar to the equivalent ratio in our experiments, the force-displacement data from an SPM measurement may not give a clear, quantitative description of the interface's adhesion properties.

The results presented in Figure 6 provide interesting insights, but the contact of multiple surface holes in Figure 7 demonstrates how surface holes can alter the adhesion of a polymer interface without the development of vacuum pockets. In Figure 7, the most striking result is the onset of force instabilities in the force-displacement

Downloaded At: 08:35 22 January 2011

curves. A force instability is a large, sudden change in the separation force with a small change in the applied displacement. During a contact adhesion test, a large sudden change in the force is attributed to a corresponding large change in the interfacial area, which is directly observed in our optical images. As the interfacial area decreases during separation, the edge of the receding contact area proceeds in sequences of stable and unstable propagation. Stable propagation, for displacement-controlled experiments, refers to the case where additional applied displacement is required to continue the movement of the contact-edge separation. If we consider this from a fracture mechanics viewpoint, stable propagation is defined as a condition when $\partial G/\partial a \geq 0$, where G is the applied energy release rate and a is the contact radius. For unstable propagation, after movement is initiated, the contact edge continues to recede without additional applied energy required (*i.e.*, $\partial G/\partial a \leq 0$). This self-driven recession continues until G becomes less than the material-defined critical energy-release rate, G_c, for failure. The reason for the transition from stable to unstable propagation is the geometry of the contact line. As the contact edge proceeds between the surface holes, the receding contact line transitions from large continuous lengths to narrow, discontinuous lengths (Figure 9). As the contact edge is confined to these narrowing regions, the applied force is distributed over a smaller crack front; therefore, the applied energy-release rate continues to increase until the contact line begins to widen. The radius and spacing of the holes dictates the rate at which the contact edge decreases, thus controlling the rate of the force instability. These results point to two important discoveries. First, similar to the single-hole experiments discussed previously, these results point to the importance of the

Downloaded At: 08:35 22 January 2011

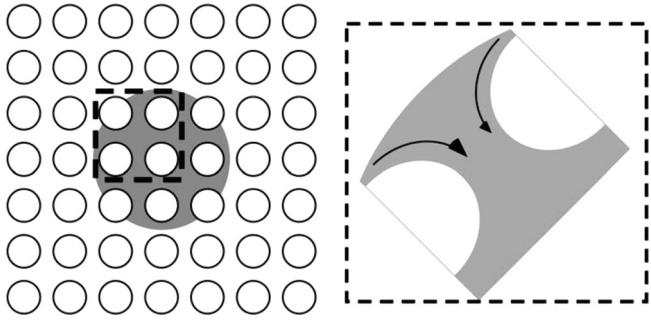

FIGURE 9 Schematic of contact line proceeding through regions that cause unstable propagation during separation. Not drawn to scale.

contact edge (or crack-tip region), not the contact area, in defining the energy required to separate an interface. Second, during unstable propagation, the contact line accelerates and decelerates as it passes from wide to narrow to wide regions. This change in the contact line velocity, or crack velocity, could be advantageous for the control of more viscoelastic polymer films. Crosslinked polydimethylsiloxane is not a strongly viscoelastic material; thus the change in crack-tip velocity does not have a large effect on G_c, or correspondingly $\overline{W}_{adh}$.

Although $\overline{W}_{adh}$ is not affected by the contact of multiple surface holes, Figure 7b shows that $\overline{P}$ is altered by the surface hole patterns. $\overline{P}$ decreases with increasing hole radius. The primary reason for this systematic decrease in the maximum separation force is the balance between the surface pattern dimensions and a critical contact radius, a_c [11,21]:

$$a_c = \left(\frac{36\pi R^2 G_c}{24E}\right)^{1/3} \tag{5}$$

This contact radius, a_c, defines the point at which the maximum separation force occurs for a nonpatterned interface of elastic materials, as predicted by the JKR theory. As discussed in a previous publication, this length scale also plays a significant role in the separation mechanism for interfaces with patterns of posts [11]. For surface hole patterns, if unstable propagation of the contact edge occurs near the radius defined by a_c, then the maximum force of separation will be less than predicted by the JKR theory. After the contact edge accelerates past a_c, it will become pinned on the next set of surface holes before finally debonding. This pinning of the contact edge gives rise to the last local maximum in the force-displacement curve. Based on this analysis, if surface hole features are not placed within the radius a_c, then at the onset of the surface hole–induced instability, complete separation would occur. This design would eliminate the second local maximum observed in the force-displacement curves. Although the total energy, as described by $\overline{W}_{adh}$ is not decreased for PDMS by the presence of surface holes, the maximum force encountered during separation can be tuned by these mechanisms.

In addition to the instabilities induced by neighboring surface holes, shallow surface holes can alter the separation mechanism by the establishment of interfacial areas at both the top and bottom of the surface holes (Figure 8). Similar to the previous discussions, this geometric configuration does not alter the value of $\overline{W}_{adh}$ for crosslinked PDMS interfaces, but it does provide a tuning mechanism for the maximum separation force. Because our experiments only involve

Downloaded At: 08:35 22 January 2011

a single spherical probe, these are the primary experiments for determining the influence of the second interfacial plane. For interfaces with single surface holes (Figure 8a), the maximum separation force increases with increasing hole radius. Although the exact mechanism causing this increase in separation force still needs to be determined, the radii for which it occurs is less than the value of a_c for the tested materials. We believe that the mechanism will be related to this material-defined length scale, but the exact interaction is yet to be revealed.

SUMMARY

Surface hole patterns provide a unique avenue for tuning the adhesion of soft polymer interfaces. The surface hole edges and their control of the contact edge dictate the stability of the separation process, thus controlling the local velocities of separation. For crosslinked PDMS, the control of local stability only impacts the maximum separation force, but it does not control the energy dissipated. It is hypothesized that this local control of separation velocities can be used advantageously for more viscoelastic polymer interfaces whose adhesion depends strongly upon separation velocity. The results discussed in this article also emphasize the importance of the contact edge in defining the adhesion of a polymer interface. Specifically for crosslinked PDMS, the results of using surface hole patterns demonstrate that the adhesion hysteresis is purely associated with phenomena that are isolated to a small volume of material near the receding contact edge. Finally, the contact adhesion results on isolated surface holes indicate the importance of observing the interfacial area morphology to correctly characterize adhesion based on contact force displacement. This result emphasizes the care that must be taken in characterizing adhesion on length scales below the limit of optical observation techniques. Overall, the surface hole patterns on crosslinked PDMS interfaces do not significantly enhance adhesion, but they do provide a robust method for tuning critical adhesion descriptors and provide an essential link in defining the general relationship between patterns, material, and adhesion.

Downloaded At: 08:35 22 January 2011

ACKNOWLEDGMENTS

The authors gratefully acknowledge the financial support of a National Science Division of Materials Research (NSF-DMR) CAREER Award, a 3M Nontenured Faculty Award, and the Center for University of Massachusetts—Industry Research on Polymers.

REFERENCES

[1] Autumn, K., Liang, Y. A., Hsieh, S. T., Zesch, W., Chan, W. P., Kenny, T. W., Fearing, R., and Full, R. J., *Nature* **405**, 681–685 (2000).
[2] Autumn, K. and Peattie, A. M., *Integr. Comp. Biol.* **42**, 1081–1090 (2002).
[3] Jagota, A. and Bennison, S. J., *Integr. Comp. Biol.* **42**, 1140–1145 (2002).
[4] Jagota, A. and Bennison, S. J., *Am. Zool.* **41**, 1483–1483 (2001).
[5] Geim, A. K., Dubonos, S. V., Grigorieva, I. V., Novoselov, K. S., Zhukov, A. A., and Shapoval, S. Y., *Nat. Mater.* **2**, 461–463 (2003).
[6] Kesel, A. B., Martin, A., and Seidl, T., *Journal of Experimental Biology* **206**, 2733–2738 (2003).
[7] Sitti, M. and Fearing, R. S., *J. Adhes. Sci. Technol.* **17**, 1055–1073 (2003).
[8] Gao, H. J. and Yao, H. M., *Proc. Natl. Acad. Sci. U.S.A.* **101**, 7851–7856 (2004).
[9] Persson, B. N. J. and Gorb, S., *J. Chem. Phys.* **119**, 11437–11444 (2003).
[10] Arzt, E., Gorb, S., and Spolenak, R., *Proc. Natl. Acad. Sci. U.S.A.* **100**, 10603–10606 (2003).
[11] Crosby, A. J., Hageman, M., and Duncan, A., *Langmuir* **21**, 11738–11743 (2005).
[12] Ghatak, A., Mahadevan, L., Chung, J. Y., Chaudhury, M. K., and Shenoy, V., *Proceedings of the Royal Society A—Mathematical, Physical and Engineering Sciences* **460**, 2725–2735 (2004).
[13] Kendall, K., *Proc. R. Soc. A* **341**, 409–428 (1975).
[14] Creton, C. and Lakrout, H., *J. Polym. Sci. Pt. B—Polym. Phys.* **38**, 965–979 (2000).
[15] Lakrout, H., Sergot, P., and Creton, C., *J. Adhes.* **69**, 307 (1999).
[16] Shull, K. R., Flanigan, C. M., and Crosby, A. J., *Physical Review Letters* **84**, 3057–3060 (2000).
[17] Crosby, A. J., Shull, K. R., Lakrout, H., and Creton, C., *J. Appl. Phys.* **88**, 2956–2966 (2000).
[18] Creton, C., Hooker, J., and Shull, K. R., *Langmuir* **17**, 4948–4954 (2001).
[19] Ghatak, A. and Chaudhury, M. K., *Langmuir* **19**, 2621–2631 (2003).
[20] Gay, C. and Leibler, L., *Phys. Rev. Letters* **82**, 936–939 (1999).
[21] Johnson, K. L., Kendall, K., and Roberts, A. D., *Proc. R. Soc. Lond. A* **324**, 301–313 (1971).
[22] Crosby, A. J. and Shull, K. R., *J. Polym. Sci. Pt. B—Polym. Phys.* **37**, 3455–3472 (1999).
[23] Creton, C. and Leibler, L., *J. Polym. Sci. P. B—Polym. Phys.* **34**, 545–554 (1996).
[24] Crosby, A. J., Shull, K. R., Lin, Y. Y., and Hui, C. Y., *J. Rheol.* **46**, 273–294 (2002).
[25] Shull, K. R., Ahn, D., Chen, W.-L., Flanigan, C. M., and Crosby, A. J., *Macromol. Chem. Phys.* **199**, 489–511 (1998).
[26] Chaudhury, M., *J. Phys. Chem. B* **103**, 6562–6566 (1999).
[27] Chaudhury, M. K. and Owen, M. J., *Langmuir* **9**, 29–31 (1993).
[28] Silberzan, P., Perutz, S., Kramer, E. J., and Chaudhury, M. K., *Langmuir* **10**, 2466–2470 (1994).
[29] Perutz, S., Kramer, E. J., Baney, J., Hui, C. Y., and Cohen, C., *J. Polym. Sci. Pt. B—Polym. Phys.* **36**, 2129–2139 (1998).
[30] Perutz, S., Kramer, E. J., Baney, J., and Hui, C. Y., *Macromolecules* **30**, 7964–7969 (1997).
[31] Andrews, E. H. and Kinloch, A. J., *Proc. R. Soc. Lond. A.* **332**, 385–399 (1973).
[32] Gent, A. N. and Petrich, R. P., *Proc. Roy. Soc. A.* **310**, 433–448 (1969).

Downloaded At: 08:35 22 January 2011